11B.2 **Impacts of evaporative cooling on tropical cyclone rainband**

Masahiro Sawada, and T. Iwasaki
Department of Geophysics, Tohoku University, Sendai, Japan

1. Introduction

Evaporative cooling has significant impacts on the development and structure of a tropical cyclone (TC) through changes of convective activity. In Sawada and Iwasaki (2010, hereafter SI2010a), it is shown that when evaporative cooling is included (control experiment) rainbands are actively formed, which produce large amounts of condensation heating at not only the eyewall but also the outside. The diabatic heating associated with rainbands greatly drives the secondary circulation of the TC and it continuously increases the kinetic energy of a TC (see, Fig. 2) and expands the TC size (e.g. radius of gale-force wind), when compared with the experiment excluding evaporative cooling (NOEVP experiment). On the other hand, in the NOEVP experiment rainbands hardly appear outside the eyewall and it retains its size very well. Roles of rainbands are considered to be important for TC characteristics because TC size is closely related with rainband activity. In spite of many observational and numerical attempts to understand the formation and propagation of rainband, the impacts of evaporative cooling on rainbands behaviors using 3D cloud-resolving simulations are not fully understood yet. Thus, herein we aim to study the formation, propagation, and maintenance mechanism of rainbands through the cloud-resolving simulations.

2. Model outline and experimental design

We use JMA-NHM developed by the Japan Meteorological Agency/Meteorological Research Institute (Saito et al. 2006). A calculation domain is 2000 km x 2000 km with a horizontal grid spacing of 2 km. The 36 vertical layers extend from the surface to a height of 24.5 km, with the lowermost layer being 40 m thick. The top and bottom are assumed to be rigid. A 2-moment, 3-ice bulk cloud microphysics scheme is incorporated.

TC simulations are conducted under a quiescent environment in which the Coriolis parameter f is assumed to be constant at 15N (f-plane). The basic state of horizontally uniform temperature and humidity profiles is given by spatially and temporally averaging the reanalysis data from the ERA-40over the subtropical region of the western North Pacific in August for five years (1998–2002). The sea surface temperature is fixed at 303 K over the whole region. An axisymmetric vortex is given at the initial condition. To clarify the roles of evaporative cooling, two experiments are carried out: one is control experiment, and the other is NOEVP experiment, which exclude evaporative cooling.

3. Results

Figure 1 shows simulated precipitation structure at T=120 h in the control and NOEVP experiment. Rainbands are actively formed

outside the eyewall in the control experiment, while they are hardly seen in the noevp one. Rainbands propagate in the counter clockwise and radially outward direction. The length of major axis of rainbands is 50-500 km, and its width is 10-50 km. The features are consistent with those by previous observational studies (Senn and Hiser 1959; Tatehira 1961; Willoughby et al. 1984; Shimazu 1997). The gale force wind area (wind speed of larger than 15ms^{-1}) is wider in the control experiment than in the NOEVP one. Strong wind area is confined around the eyewall area in the NOEVP experiment.

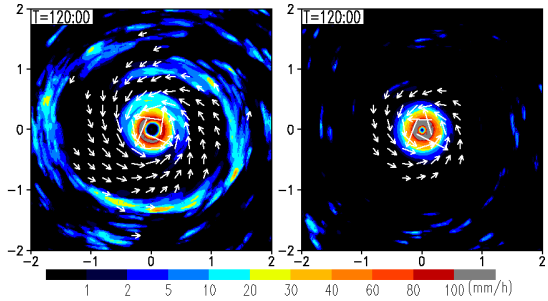

Fig. 1 Precipitation pattern at T=120 h in the control (left) and NOEVP (right) experiments. Vectors show horizontal wind speed of larger than 15 ms^{-1}.

To see the basic structure of simulated TC, time-series of central sea-level pressure (CSLP) and area-averaged kinetic energy are shown in Fig. 2. In the both experiments, CSLP starts to deepen T=36 h and it reaches about 935 hPa at T=72 h in the control experiment and 910 hPa at T=48 h in the NOEVP one. A rapid intensification of NOEVP experiment is caused by large convective available potential energy around the eyewall associated with the absence of evaporative cooling (SI2010a). In the control experiment, the kinetic energy gradually increases with time and exceeds that of NOEVP experiment. The kinetic energy keeps an almost constant in the NOEVP after rapid intensification (T=48 h). The result indicates evaporative cooling also leads to a significant difference in kinetic energy.

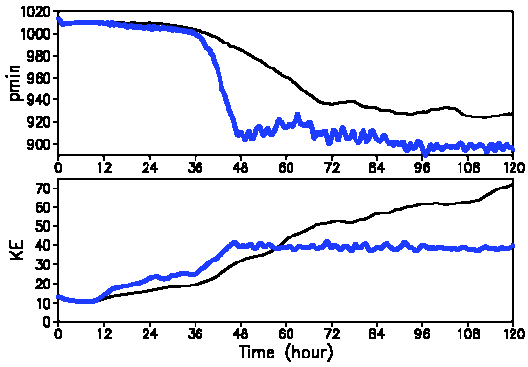

Fig. 2 Time evolutions of central sea-level pressure (top) and area-averaged kinetic energy within a radius of 300 km from the TC center (bottom). Black line is control experiment and blue is NOEVP one.

To examine the time tendency of the location of organized convection (rainband and eyewall), azimuthally averaged precipitation is plotted in both experiments, as shown in Fig. 3. A vertically and azimuthally averaged tangential wind is also shown to display the size of the strong wind area. For the precipitation, an outward propagation of an active convection region is observed in the control experiment. This corresponds to outward propagation of rainbands produced by cold pools and downdrafts associated with evaporative cooling, which play important roles in the convection initiation and the maintenance of convective cells. On the other hand, in the NOEVP experiment the outward propagation of precipitation is hardly seen because of the absence

of cold pools and downdrafts.

The tangential wind shows the radius of a strong wind region (larger than 15 ms^{-1}) expands gradually to about 180 km at T=120 h, which indicates that a TC continues to develop even if it reaches its mature stage defined by a tendency of the CSLP. In contrast, in the NOEVP experiment the strong wind region is formed more quickly than in the control experiment. The radius of the strong wind region becomes about 120 km at T=30 h, and its size remains almost unchanged. The time tendencies of the radius of strong wind region are consistent with those of the area-averaged kinetic energy.

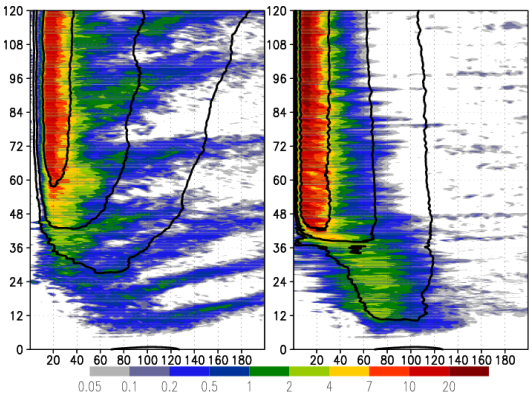

Fig. 3 Time-radius cross-sections of azimuthally averaged rain rate (color) and tangential wind vertically averaged from surface to z=5.14 km (contour), with contour values of 15, 25, and 50 ms^{-1} in the control (left) and NOEVP (right) experiments.

The formation and propagation of rainband are closely related to cold pools produced by evaporative cooling. Figure 4 illustrates detailed processes of simulated rainband. Cold pools appear markedly below the convective cells in the middle panel. They are formed by evaporative cooling from raindrops. Cold pools produce horizontal convergences at the near surface between the upstream side of cold pools and low-level inflows along streamlines, and its lifting forms new convective cells. New convective cells are successively generated at the upstream end of an old convective cell, which are organized into the spiral-shaped rainband along the low-level, azimuthally averaged streamlines. This formation process is called hereafter as the upstream development. The upstream development propagates spiral-shaped rainband radially outward. Thus, cold pools play an essential role in the upstream development.

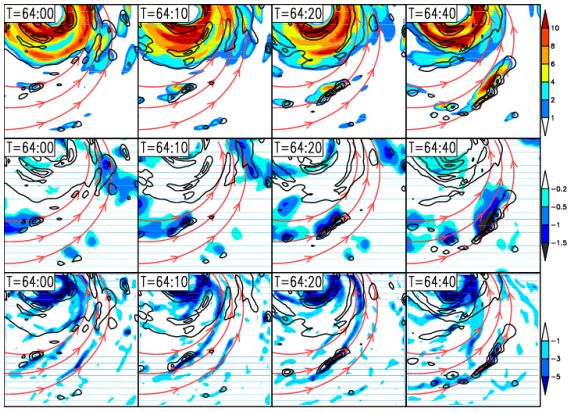

Fig. 4 Contours depict horizontal distribution of rainwater with contour values of 2, 10, and 30 kgm^2. Colored areas display rain rate (top), potential temperature anomaly from an azimuthally averaged temperature at 20-m height (middle), and horizontal convergence (bottom). Red solid lines with arrows are streamlines azimuthally and temporally averaged at a height of 260 m.

Cold pool also induces pressure anomaly near the surface and it causes asymmetric flows from azimuthally averaged low-level wind. The

asymmetric flows advance cold pool fronts, in the normal direction to rainbands, called hereafter as cross-band propagation. The cross-band propagation deflects movement of each cell away from the low-level streamlines and rotates it in the counter clockwise direction. Cross-band propagation is favorable movement for maintenance of convective cells, giving a positive feedback to the maintenance of rainbands.

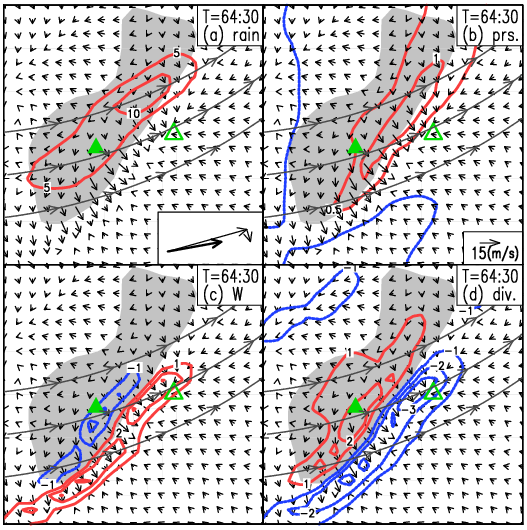

Fig. 5 Cold pool (shaded area) and rainband. Contour shows (a) precipitation, (b) vertical motion at z=620 m, (c) pressure anomaly from azimuthally averaged pressure at z=20 m, and (d) horizontal divergence at z=20 m. Dashed lines are negative values. Vectors present wind anomaly from azimuthally averaged wind at z=260 m.

4. Conclusion

Evaporative cooling produces radially outward propagation of rainbands through cold pool dynamics, which expands the TC size through enhanced secondary circulation associated with condensation heating of precipitation outside the eyewall. In contrast, they are hardly observed in the NOEVP experiment. At least, the rainbands features in this study seem to be more closely related to cold pool dynamics than the proposed mechanisms for rainband formation and propagation by previous studies (internal gravity waves and vortex Rossby waves). Rainband behaviors result from upstream development and cross-band propagation, which are quite similar to those of the observed radar echo patterns (Tatehira 1961).

References

Saito, K., and Coauthors, 2006: The operational JMA nonhydrostatic mesoscale model. Mon. Wea. Rev., 134, 1266–1298.

Sawada, M., and T. Iwasaki, 2010: Impacts of evaporation from raindrops on tropical cyclones. Part I: Evolution and Axisymmetric structure. J. Atmos. Sci., 67, 71–83.

——, and ——, 2010: Impacts of evaporation from raindrops on tropical cyclones. Part II: Features of rainbands and asymmetric structure. J. Atmos. Sci., 67, 84–96.

Senn, H. V., and H. W. Hiser, 1959: On the origin of hurricane spiral rainbands. J. Atmos. Sci., 16, 419–426.

Shimazu, Y., 1997: Wide slow-moving rainbands and narrow fastmoving rainbands observed in Typhoon 8913. J. Meteor. Soc. Japan, 75, 67–80.

Tatehira, R., 1961: Radar and mesoscale analysis of rainband in typhoon—Case study of Typhoon Helen (No. 5821) (in Japanese). J. Meteor. Res., 13, 264–279.

Willoughby, H. E., F. D. Marks Jr., and R. J. Feinberg, 1984: Stationary and moving convective bands in hurricanes. J. Atmos. Sci., 41, 3189–3211.